

Solidification and Crystallization

Edited by

Dieter M. Herlach

DGM



Solidification and Crystallization

Edited by

Dieter M. Herlach

DGM



Related Titles from Wiley-VCH

H.-P. Degischer, B. Kriszt (Eds.)

Handbook of Cellular Metals

2002

ISBN 3-527-30339-1

G. Kostorz

Phase Transformations in Materials

2001

ISBN 3-527-30256-5

K. U. Kainer (Ed.)

Magnesium Alloys and Technology

2003

ISBN 3-527-30570-X

C. Leyens, M. Peters (Eds.)

Titanium and Titanium Alloys

2003

ISBN 3-527-30534-3

Solidification and Crystallization

Edited by
Dieter M. Herlach

DGM



WILEY-VCH Verlag GmbH & Co. KGaA

Edited by

Prof. Dieter M. Herlach

DLR – German Aerospace Center
Institute of Space Simulation
51170 Köln
Germany

All books published by Wiley-VCH are carefully produced. Nevertheless, authors, editors, and publisher do not warrant the information contained in these books, including this book, to be free of errors. Readers are advised to keep in mind that statements, data, illustrations, procedural details or other items may inadvertently be inaccurate.

Library of Congress Card No.: applied for

British Library Cataloguing-in-Publication

Data: A catalogue record for this book is available from the British Library.

Bibliographic information published by

Die Deutsche Bibliothek

Die Deutsche Bibliothek lists this publication in the Deutsche Nationalbibliografie; detailed bibliographic data is available in the Internet at <<http://dnb.ddb.de>>

© 2004 WILEY-VCH Verlag GmbH & Co. KGaA, Weinheim,

All rights reserved (including those of translation into other languages). No part of this book may be reproduced in any form – by photoprinting, microfilm, or any other means – nor transmitted or translated into machine language without written permission from the publishers. Registered names, trademarks, etc. used in this book, even when not specifically marked as such, are not to be considered unprotected by law.

Printed in the Federal Republic of Germany
Printed on acid-free paper

Composition ProSatz Unger, Weinheim
Printing betz-druck GmbH, Darmstadt
Bookbinding Großbuchbinderei J. Schäffer GmbH & Co. KG, Grünstadt

ISBN 3-527-31011-8

Preface

The Federation of European Materials Societies (FEMS) organized the biannual meeting of EUROMAT conference 2003 in Lausanne, Switzerland. This conference was essentially focussed on materials development and application. One of the conference topic was dedicated to *PHASE TRANSFORMATION* chaired by Professor Wilfried Kurz, Lausanne. It consisted of two symposia S1 on *SOLIDIFICATION* and S3 on *SOLID STATE TRANSFORMATION*.

Papers submitted originally to Symposium S2 *MODELLING* were integrated into Symposium S1. All together 96 abstracts not only from Europe but also from Asia and America were submitted to Symposium S1 with which S1 became the largest symposium of EUROMAT 2003 conference. The papers were distributed to three sessions on *Modelling*, two sessions on *Microstructures* and one session on *Properties of Melts, Nucleation, Dendritic Growth, Phase Selection, Multiphase Alloys and Processing Methods*, respectively. In addition there was a poster session.

The symposium was started with a plenary lecture by Professor Michel Rappaz on *Modelling of Solidification with Special Emphasis on the Last Stage Solidification*. The oral sessions and the poster session attracted many attendees and experienced vivid discussions showing that the research area of solidification is carried by a large and very active scientific community. In particular, remarkable progress was reported on new experimental methods and techniques for direct observation and analysis of solidification pathways both under near- and non-equilibrium conditions. Simultaneously, modelling of solidification proceeded to a big step forwards enabling now even the computer assisted description of solidification phenomena in multiphase and multicomponent alloys. Such progress is of fundamental interest for materials science but also very important in developing innovative techniques in materials production routes of improved efficiency in casting processes of foundry industry. Since by far most of the materials are produced from the liquid state as their parent phase even small but steady advances in solidification processing leads to correspondingly large consequences in progress of economy and living conditions of daily human life. It is therefore mandatory for a prosperous society.

The present Publications to EUROMAT 2003 contains selected papers of symposium S1 which have been invited for submission to publication in the present book. Each manuscript was peer reviewed by two independent experts before acceptance for publication. Certainly, the peer review process has essentially contributed to the

quality of the present volume. I appreciate the valuable and important assistance of all experts who delivered reports on submitted manuscripts.

I would like to extend my gratitude to Professor Wilfried Kurz for inviting me as an organizer of the symposium *Solidification* of the topic of *Phase Transformation*, and the colleagues who took over the chairmanship of the different sessions as Andreas Ludwig (Leoben), Michel Rappaz (Lausanne), Heike Emmerich (Dortmund), A. Lindsay Greer (Cambridge), Heiner Müller-Krumbhaar (Jülich), Dirk Holland-Moritz (Köln), Andy Mullis (Leeds), Lorenz Ratke (Köln), Peter Schuhmacher (Leoben) and Britta Nestler (Karlsruhe). I enjoyed the cooperation with Michel Rappaz in his help of combining Symposium S2 (Modelling) with Symposium S1 (Solidification). My thanks are to the local organisers in Lausanne for an excellent conference performance, Peter-Paul Schepp from the Deutsche Gesellschaft für Materialkunde in the preparation of the programme, the Deutsche Forschungsgemeinschaft for support within the priority program SPP1120 and Jörn Ritterbusch and Jörg Wrzesinski from WILEY-VCH for their great help in editing this book.

Köln, August 2004

Dieter M. Herlach
Organizer of Symposium
Solidification of EUROMAT 2003

Contents

| | | |
|----------|---|-----------|
| | Preface | V |
| 1 | Complex Structures: A Symbiosis of Experiments and Numerical Studies | 1 |
| | J. H. BILGRAM and H. M. SINGER | |
| | Abstract | 1 |
| 1.1 | Introduction | 1 |
| 1.2 | Experimental Studies | 2 |
| 1.3 | Numerical Studies | 5 |
| 1.4 | Conclusions | 6 |
| | Acknowledgements | 7 |
| | References | 7 |
| 2 | Thermal Roughening of a Solid-on-Solid Model with Elastic Interaction | 9 |
| | FRANK GUTHEIM, HEINER MÜLLER-KRUMBHAAR, EFIM BRENER and CHRISTOPH PÜTTER | |
| 2.1 | Introduction | 9 |
| 2.2 | Step Interaction | 9 |
| 2.3 | Model Description | 10 |
| 2.4 | Results and Discussion | 13 |
| 2.4.1 | Height Correlation Function | 13 |
| 2.4.2 | Energetic Scales | 14 |
| 2.4.3 | Average Energy | 14 |
| 2.4.4 | Defect Correlations | 14 |
| 2.4.5 | Line Energy vs. Step Interaction | 15 |
| 2.4.6 | Crystal Growth | 15 |
| 2.5 | Conclusion | 16 |
| | References | 16 |
| 3 | A Phase-Field Model for Crystallization into Multiple Grain Structures | 17 |
| | HAMID ASSADI | |
| | Abstract | 17 |
| 3.1 | Introduction | 17 |

| | | |
|----------|--|-----------|
| 3.2 | Theoretical Background and Model Development | 18 |
| 3.3 | Simulations | 21 |
| 3.3.1 | Temperature Dependence of Interfacial Energy | 22 |
| 3.3.2 | Crystallization by Inoculation | 22 |
| 3.3.3 | Crystallization by Homogeneous Nucleation | 24 |
| | References | 26 |
| 4 | Scaling Relations for Dendritic Solidification in Binary Alloys | 27 |
| | HEIKE EMMERICH, MATTHIAS JURGK, RICARDO SIQUIERI | |
| 4.1 | Introduction | 27 |
| 4.2 | Two-scale Modeling for Binary Alloys | 28 |
| 4.3 | A Novel Scaling Relation Taking into Account Crystal Density | 30 |
| 4.4 | Numerical Investigations of the Two-scale Model | 31 |
| | Summary | 32 |
| | References | 33 |
| 5 | Modeling the Spatial Phase Separation Process in Hypermonotectic Alloys | 34 |
| | M. WU, A. LUDWIG, L. RATKE | |
| | Abstract | 34 |
| 5.1 | Introduction | 34 |
| 5.2 | Numerical Model | 35 |
| 5.2.1 | Phase Definition | 35 |
| 5.2.2 | Conservation equations | 35 |
| 5.2.3 | Droplet Growth and Mass Transfer | 36 |
| 5.2.4 | Marangoni Force and Hydrodynamic Resistance | 37 |
| 5.3 | Problem description | 38 |
| 5.4 | Results and Discussions | 39 |
| 5.4.1 | Without Gravity | 39 |
| 5.4.2 | With Gravity | 40 |
| 5.5 | Conclusions | 42 |
| | References | 42 |
| 6 | Modeling of the Solidification of Immiscible Alloys | 44 |
| | J. Z. ZHAO, Z. Q. HU, L. RATKE | |
| | Abstract | 44 |
| 6.1 | Introduction | 44 |
| 6.2 | Theoretical Model | 45 |
| 6.3 | Numerical Results and Discussions | 48 |
| 6.4 | Conclusions | 51 |
| | Acknowledgments | 51 |
| | References | 51 |

| | | |
|-----------|---|-----------|
| 7 | Phase-Field Modeling of Dendritic Solidification: Verification for the Model Predictions with Latest Experimental Data | 52 |
| | P.K. GALENKO, D.M. HERLACH, O. FUNKE, G. PHANIKUMAR | |
| | Abstract | 52 |
| 7.1 | Introduction | 52 |
| 7.2 | Governing equations | 53 |
| 7.3 | Results and Discussion | 55 |
| 7.3.1 | Dendritic Patterns | 56 |
| 7.3.2 | Comparison with experimental data | 57 |
| 7.4 | Conclusions | 58 |
| | Acknowledgements | 59 |
| | References | 59 |
| 8 | Phase-Field Modeling of Phase Transitions in Ternary Alloys | 61 |
| | BRITTA NESTLER | |
| 8.1 | Introduction | 61 |
| 8.2 | Phase-Field Model | 62 |
| 8.3 | Phase Transitions of Ternary Alloys | 64 |
| 8.4 | Outlook | 68 |
| | Acknowledgements | 69 |
| | References | 69 |
| 9 | Modeling of Heat and Solute Flows during Solidification of Droplets | 70 |
| | R. HERINGER, CH.-A. GANDIN, G. LESOULT, H. HENEIN | |
| | Abstract | 70 |
| 9.1 | Introduction | 70 |
| 9.2 | Experimental | 71 |
| 9.3 | Modeling | 72 |
| 9.3.1 | Macroscopic Heat and Solute Flows | 72 |
| 9.3.2 | Front Tracking and Growth Velocity | 73 |
| 9.3.3 | Microsegregation and Mushy Zone Solidification | 74 |
| 9.3.4 | Initial and Boundary Conditions, Numerical Implementation | 75 |
| 9.4 | Results | 76 |
| 9.5 | Concluding Remarks | 80 |
| | Acknowledgements | 81 |
| | References | 81 |
| 10 | Thermo-physical and Physical Properties for Use in Solidification Modelling of Multi-component Alloys | 82 |
| | N. SAUNDERS, Z. GUO, A. P. MIODOWNIK and J-PH. SCHILLÉ | |
| | Abstract | 82 |
| 10.1 | Introduction | 82 |
| 10.2 | Technical Background | 84 |
| 10.2.1 | The Scheil-Gulliver Approach with Modification for fast C and N Diffusion | 84 |

| | | |
|-----------|---|------------|
| 10.2.2 | Modelling of Physical Properties | 87 |
| 10.3 | Example Calculations | 88 |
| 10.3.1 | Variations in Behaviour Within an Alloy Composition Specification Range | 88 |
| 10.3.2 | Behaviour of the Liquid in the Mushy Zone | 90 |
| 10.4 | Discussion | 93 |
| 10.5 | Summary and Conclusions | 93 |
| | References | 94 |
| 11 | Determination of Solidification Curves Based on DSC Experiments with Improved Heat-transfer Model | 95 |
| | DJORDJE MIRKOVIĆ, JOACHIM GRÖBNER, RAINER SCHMID-FETZER | |
| 11.1 | Introduction | 95 |
| 11.2 | DSC Experiment and Heat-Transfer Model (DSC-HTM) | 96 |
| 11.2.1 | DSC Experiment | 96 |
| 11.2.2 | Heat-transfer Model | 96 |
| 11.3 | Solidification Curves Determined by Alternative Methods | 99 |
| 11.3.1 | Quenching and Image Analysis (QIA) | 99 |
| 11.3.2 | Thermodynamic Calculation of Solidification Curves | 99 |
| 11.4 | Results and Discussion | 100 |
| | Acknowledgement | 102 |
| | References | 102 |
| 12 | Measurement of the Surface Tension of Undercooled Melts by the Oscillating Drop Method in an Electrostatic Levitator | 103 |
| | PETER L. RYDER and NILS WARNCKE | |
| 12.1 | Introduction | 103 |
| 12.2 | Experimental Methods | 104 |
| 12.2.1 | The Levitator | 104 |
| 12.2.2 | The Oscillating Drop Method | 105 |
| 12.2.2.1 | Principle | 105 |
| 12.2.2.2 | Excitation and Detection of the Oscillations | 105 |
| 12.3 | Results | 106 |
| 12.4 | Summary and Conclusions | 109 |
| | Acknowledgements | 109 |
| | References | 109 |
| 13 | Liquid-liquid Interfacial Tension and Wetting in Immiscible Al-based Systems | 110 |
| | WALTER HOYER, IVAN KABAN, MARKUS MERKWITZ | |
| 13.1 | Introduction | 110 |
| 13.2 | Experimental Technique | 110 |
| 13.3 | Results and Discussion | 113 |
| 13.4 | Conclusions | 117 |
| | Acknowledgements | 118 |

| | | |
|-----------|---|------------|
| | References | 118 |
| 14 | In-Situ Optical Determination of Fraction Solid | 119 |
| | L. RATKE, D. TSCHUSCHNER | |
| | Abstract | 119 |
| 14.1 | Introduction | 119 |
| 14.2 | Experimental | 120 |
| 14.3 | Experimental Results | 121 |
| 14.4 | Mathematical Analysis of the Intensity Curves | 122 |
| 14.5 | Fraction Solid | 124 |
| 14.6 | Discussion and Conclusion | 125 |
| | References | 127 |
| 15 | Magnetic Effects on the Nucleation in Undercooled Co-Pd Melts | 128 |
| | DIRK HOLLAND-MORITZ AND FRANS SPAEPEN | |
| 15.1 | Introduction | 128 |
| 15.2 | Classical Approach to Describe the Nucleation Behavior of Co-Pd Melts | 129 |
| 15.3. | Extension of the Classical Nucleation Model by Magnetic Contributions | 132 |
| 15.4. | Conclusions | 135 |
| | Acknowledgements | 135 |
| | References | 136 |
| 16 | Identification of the Substrate of Heterogeneous Nucleation in Zn-Al Alloy Inoculated with ZnTi-Based Master Alloy | 137 |
| | WITOLD K. KRAJEWSKI, A. LINDSAY GREER, THOMAS E. QUESTED, WALDEMAR WOLCZYNSKI | |
| | Abstract | 137 |
| 16.1 | Introduction | 137 |
| 16.2 | Experimental Methods | 138 |
| 16.3 | Results and Discussion | 140 |
| 16.3.1 | Thermal Analysis and Structure | 140 |
| 16.3.2 | Crystal Structure and Chemical Composition | 142 |
| 16.3.3 | Crystal orientation | 144 |
| 16.3.3.1 | TEM Examination of Thin Foils | 144 |
| 16.3.3.2 | SEM – EBSD Examinations | 144 |
| 16.4 | Conclusions | 146 |
| | Acknowledgements | 147 |
| | References | 147 |

| | | |
|-----------|---|------------|
| 17 | Undercooling and Solidification of Liquid Silicon | 148 |
| | C. PANOFEN, R. P. LIU, D. HOLLAND-MORITZ, T. VOLKMANN, D.M. HERLACH | |
| 17.1 | Abstract | 148 |
| 17.2 | Introduction | 148 |
| 17.3 | Experimental | 149 |
| 17.4 | Results & Discussion | 151 |
| 17.4.1 | Surface Morphologies and Solidification Mode | 151 |
| 17.4.2 | Growth Velocity Results | 153 |
| 17.5 | Conclusion | 155 |
| | Acknowledgements | 155 |
| | References | 155 |
| | | |
| 18 | Two-Phase Equilibrium in Binary Alloy Nano Particles | 157 |
| | P. BUNZEL, G. WILDE, H. RÖSNER, J. WEISSMÜLLER | |
| 18.1 | Introduction | 157 |
| 18.2 | Idealized Model System | 158 |
| 18.2.1 | The Model Alloy | 158 |
| 18.2.2 | Particle Shape and Properties of the Phase Boundary | 159 |
| 18.2.3 | Surface Area of the Phase Boundary | 159 |
| 18.2.4 | Molar Free Energies | 160 |
| 18.3 | Size-dependent Alloy Phase Diagrams | 161 |
| 18.4 | Conclusion | 164 |
| | Acknowledgement | 165 |
| | References | 165 |
| | | |
| 19 | Three-dimensional Reconstruction of Experimentally Grown Xenon Dendrites | 166 |
| | H.M. SINGER and J.H. BILGRAM | |
| 19.1 | Introduction | 166 |
| 19.2 | Experimental Setup | 167 |
| 19.3 | Analytical Models vs. Simulations | 168 |
| 19.4 | Reconstruction | 169 |
| 19.5 | Results and Discussion | 172 |
| | References | 173 |
| | | |
| 20 | Mechanically Deformed Primary Dendritic Structures Observed During the Solidification of Undercooled Melts | 175 |
| | ANDREW M. MULLIS, KALIN DRAGNEVSKI, & ROBERT F. COCHRANE | |
| 20.1 | Introduction | 175 |
| 20.2 | Experimental Method | 177 |
| 20.3 | Experimental Evidence for Deformed Dendritic Structures | 178 |
| 20.4 | Discussion | 179 |
| 20.5 | Summary & Conclusions | 183 |
| | References | 183 |

| | | |
|-----------|---|------------|
| 21 | Effect of Hydrodynamics on Microstructure Evolution of Nd-Fe-B Alloys | 185 |
| | R. HERMANN, G. GERBETH, O. FILIP, J. PRIEDE, V. SHATROV | |
| | Abstract | 185 |
| 21.1 | Introduction | 185 |
| 21.2 | Experimental | 186 |
| 21.3 | Results | 187 |
| 21.3.1 | Levitation | 187 |
| 21.3.2 | Magnetic Two-phase Stirrer | 190 |
| 21.4 | Conclusions | 192 |
| | Acknowledgements | 193 |
| | References | 193 |
| | | |
| 22 | Effect of the Fluid Convection Driven by a Rotating Magnetic Field on the Solidification of a PbSn Alloy | 194 |
| | B. WILLERS, S. ECKERT, U. MICHEL, G. ZOUHAR | |
| 22.1 | Introduction | 194 |
| 22.2 | Experimental Procedure | 195 |
| 22.3 | Discussion of the Results | 197 |
| 22.3.1 | Thermal analysis | 197 |
| 22.3.2 | UDV Measurements | 199 |
| 22.3.3 | Microstructure | 200 |
| 22.4 | Discussion, Conclusions | 202 |
| | Acknowledgement | 202 |
| | References | 203 |
| | | |
| 23 | Grain Sedimentation and Melt Convection Phenomena During Globular Equiaxed Solidification | 204 |
| | M. WU, A. LUDWIG and A. BÜHRIG-POLACZEK | |
| 23.1 | Introduction | 204 |
| 23.2 | Brief Description of the Numerical Model | 205 |
| 23.3 | Experimental procedure | 207 |
| 23.4 | Results and discussions | 208 |
| 23.5 | Conclusions and outlook | 211 |
| | Acknowledgments | 212 |
| | References | 212 |
| | | |
| 24 | Metastable Primary Solidification Modes in the Fe-Cr-Ni System During Laser Welding | 213 |
| | H. SCHOBERT, TH. BÖLLINGHAUS, M. WOLF | |
| | Abstract | 213 |
| 24.1 | Introduction | 213 |
| 24.2 | Ferrite – Austenite Type of Primary Solidification Change | 214 |
| 24.3 | Geometric Analysis of Solidification Structures | 218 |
| 24.4 | Metastable States and Epitaxial Effects at the Fusion Line | 222 |
| 24.5 | Metastable Ferritic Solidification | 223 |

| | | |
|-----------|---|------------|
| 24.6 | Conclusions | 225 |
| | References | 226 |
| 25 | Crystallization of the Nd₂Fe₁₄B Peritectic Phase from the Undercooled Melt by Containerless Processing | 227 |
| | SHUMPEI OZAWA, MINGJUN LI, SUGURU SUGIYAMA, ITARU JIMBO and KAZUHIKO KURIBAYASHI | |
| 25.1 | Introduction | 227 |
| 25.2 | Experimental Procedure | 228 |
| 25.3 | Results | 228 |
| 25.3.1 | Nd _{11.8} Fe _{82.3} B _{5.9} (Nd ₂ Fe ₁₄ B) Alloy | 228 |
| 25.3.2 | Nd ₁₄ Fe ₇₉ B ₇ Alloy | 231 |
| 25.4 | Discussions | 234 |
| 25.5 | Conclusion | 237 |
| | Acknowledgements | 237 |
| | References | 238 |
| 26 | Thermomagnetic Analyses of Nd-Fe-B Bulk Alloys Solidified from the Undercooled Melt | 239 |
| | S. REUTZEL, T. VOLKMANN, J. GAO, J. STROHMENGER, D.M. HERLACH | |
| | Abstract | 239 |
| 26.1 | Introduction | 239 |
| 26.2 | Experimental | 240 |
| 26.3 | Results and Discussion | 241 |
| 26.4 | Summary | 248 |
| | Acknowledgements | 248 |
| | References | 249 |
| 27 | Analysis of the Solidification Microstructure of Multi-component Gamma Titanium Aluminide Alloys | 250 |
| | VIOLA KÜSTNER, MICHAEL OEHRING, ANITA CHATTERJEE, HELMUT CLEMENS, FRITZ APPEL | |
| 27.1 | Introduction | 250 |
| 27.2 | Experiments | 251 |
| 27.3 | Results | 251 |
| 27.4 | Discussion | 255 |
| 27.5 | Conclusions | 257 |
| | Acknowledgements | 257 |
| | References | 257 |
| 28 | Formation of Eutectic Cells in Ternary Al-Cu-Ag Alloys | 259 |
| | ULRIKE HECHT, VICTOR WITUSIEWICZ, ANNE DREVERMANN, STEPHAN REX | |
| 28.1 | Introduction | 259 |
| 28.2 | Experimental Procedure | 260 |
| 28.2.1 | Sample Material | 260 |

| | | |
|-----------|---|------------|
| 28.2.2 | Solidification Process and Sample Analysis | 260 |
| 28.3 | Experimental Results | 261 |
| 28.3.1 | Planar Coupled Growth | 262 |
| 28.3.2 | Cellular Coupled Growth: Elongated and Regular Cells | 264 |
| 28.4 | Discussion of the Process of Cell Formation | 267 |
| 28.5 | Summary and Outlook | 269 |
| | Acknowledgements | 270 |
| | References | 270 |
| 29 | Lamellar Pattern Formation during 2D-Directional Solidification of Ternary Eutectic Alloys | 271 |
| | MARKUS APEL, BERND BÖTTGER, VICTOR WITUSIEWICZ, ULRIKE HECHT, INGO STEINBACH | |
| 29.1 | Introduction | 271 |
| 29.2 | Phase Field Model | 271 |
| 29.2.1 | Material Data | 273 |
| 29.2.2 | Numerical Aspects and Simulation Procedure | 274 |
| 29.3 | Simulation Results | 275 |
| 29.3.1 | The Basic State and Tilted Growth | 275 |
| 29.3.2 | Higher Order Stacking Sequences and Axisymmetric Growth | 277 |
| 29.4 | Discussion and Summary | 277 |
| | Acknowledgement | 278 |
| | References | 279 |
| 30 | Simulation of Stray Grain Formation in Investment Cast Turbine Blades | 280 |
| | X. L. YANG, H. B. DONG, W. WANG and P. D. LEE | |
| | Abstract | 280 |
| 30.1 | Introduction | 280 |
| 30.2 | Model Description | 281 |
| 30.3 | Simulation Parameters | 282 |
| 30.4 | Results and Discussion | 283 |
| 30.4.1 | Effect of Withdrawal Velocity and Isothermal Conditions on Undercooling | 283 |
| 30.4.2 | Dendritic Growth and Stray Grain Formation | 284 |
| 30.4.3 | Effect of Withdrawal Velocity on Stray Grain Formation | 286 |
| 30.4.4 | Effect of Inclination Angle of Isotherms on Stray Grain Formation | 287 |
| 30.5 | Conclusions | 288 |
| | Acknowledgements | 288 |
| | References | 288 |
| 31 | Laser Cladding Applications to Combinatorial Materials Science | 290 |
| | R. VILAR, P. CARVALHO, R. COLAÇO | |
| | Abstract | 290 |
| 31.1 | Introduction | 290 |

| | | |
|-----------|--|------------|
| 31.2 | Laser Assisted Synthetic Methods | 292 |
| 31.3 | Examples of Application | 293 |
| 31.3.1 | Structure and Properties of Ni-Al-Co Alloys | 293 |
| 31.3.2 | Metal-matrix-composites for Wear-resistant Coatings | 295 |
| 31.4 | Conclusions | 298 |
| | References | 298 |
| 32 | Control of Morphological Features in Micropatterned Ultrathin Films | 300 |
| | E. MEYER, H.-G. BRAUN | |
| | Abstract | 300 |
| 32.1 | Introduction | 300 |
| 32.2 | Experimental | 301 |
| 32.3 | Results and Discussion | 301 |
| 32.4 | Perspectives | 307 |
| | Acknowledgement | 308 |
| | References | 308 |
| | Author Index | 311 |
| | Subject Index | 313 |

1

Complex Structures: A Symbiosis of Experiments and Numerical Studies

J. H. BILGRAM and H. M. SINGER

Abstract

Dendrites are the best studied structures formed during solidification of undercooled melt. Additionally other complex structures have been found in experiments and numerical studies. We perform 2D/3D-numerical simulations of solidification processes and experiments which allow *in situ* investigations of three-dimensional growth of xenon crystals into undercooled pure melt. Dendrites, seaweed, doublons, triplons etc. can be produced in experiments and numerical studies depending on initial conditions. In an interplay of numerical studies and experiments we use simulations to interpret and to plan experiments. Experimental results are used as a basis of model calculations and the development of models of complex shapes. Three-dimensional growth shapes of crystals are reconstructed using sophisticated image processing combined with experimentally determined shape parameters.

1.1

Introduction

Applications in automotive industry call for aluminium castings to be mass-produced without casting defects. Predictive models are necessary to prevent such defects. During the growth of a solid from its undercooled parent melt microstructures are formed. The best-known cases of such structures are dendrites. Microstructural changes can be observed as undercooling is increased, namely the typical length scales like the tip radius decrease with increasing undercooling [1, 2]. These are quantitative changes. In addition to that, for some materials it has been observed that they also undergo an abrupt decrease in microscale with increasing undercooling. This effect is known as spontaneous grain refinement. It has been observed in solidification from undercooled pure metallic melts [3] and alloys [4, 5]. Evidence has been found that spontaneous grain refinement is initiated by changes in the morphology of the microscopic structures [3]. This is in difference to the above mentioned quantitative grain refinement with increasing undercooling. In order to obtain more information on shapes, developed during solidification, numerical modeling and analytical stu-

dies of the solidification process have been performed. Starting with a mathematical formulation of the dendrite problem, the goal is to find out which solutions exist and which morphologies are possible. Namely the stability of solutions has been studied [6, 7, 8]. A very astonishing result was the discovery of a doublon in 2D studies [9]. It is formed by two crystalline tips with a straight channel in between. This is a typical non-equilibrium shape. It was followed up by numerical studies which found a triplet in an 3D channel [8]. In a next step a morphology diagram has been developed for 2D systems [10, 11]. Regions for stable fractal and compact growth of dendrites and seaweed have been determined. Seaweed has been considered to be built up from doublons. In this study the stability regions of morphologies have been determined in a field of supercooling of the melt vs. anisotropy of the surface free energy. Supercooling is given in the range from 0 to 1 in dimensionless units and the anisotropy in the range from 0 to 1. High anisotropies lead to dendritic growth, at low anisotropy and sufficient undercooling seaweed is growing. The amount of noise in the system under consideration may influence the position of the phase boundaries. Therefore the phase diagram has to be considered to be a qualitative one.

To verify predictions, numerical and experimental studies have to be combined. We hope that such combined studies will stimulate the application of theoretical results in the design casting processes.

1.2

Experimental Studies

Existing models for dendritic growth do not predict morphological parameters with sufficient accuracy for reliable calculations to be applied in industrial casting processes. Metallographic techniques show microstructures which have been transformed during solidification and subsequent cooling. The study of decanted structures leads to an overestimation of the fraction of solid and does not provide information of solidification kinetics. Time resolved synchrotron radiation imaging techniques do not provide a lateral resolution sufficient to determine typical length scales of the fine structure and it is not possible to study three-dimensional structures with this technique up to now [12]. Thus the use of transparent materials is the only way to determine growth parameters of morphologies during the solidification process. Two types of experiments have been performed: quasi two dimensional studies on organic alloys [13] and studies of pure materials during free growth in three dimensions [14, 15, 16].

First experimental evidence of doublons has been achieved by Akamatsu et al. [13]. A thin cuvette was used and the material was an mixture of two organic liquids CBr_4 and C_2Cl_6 . This system has two properties, which are important for the experiment:

- i) An alloy is used. It is well known that in alloys much higher constitutional undercoolings are possible than for bulk undercoolings in a pure melt.
- ii) Interface kinetics and surface free energy of the solid-liquid interface are anisotropic. Therefore this system has the great advantage that it is possible to change anisotropy of the surface free energy by changing the orientation of the seed crystal.

In these experiments the growth of seaweed has been observed and phase diagrams of the type as developed by Brener et al. [11] have been verified.

The calculations of Brener et al. have been performed for a 2D system. The experiments of Akamatsu et al. have been performed in a thin cuvette and thus it is a quasi-two-dimensional system. A two-dimensional doublon is topologically different from a doublon in three dimensions, because in 2D there is only one way out of the channel, namely at the tips. In the 3D case it is possible to move out of the channel in a direction perpendicular to the plane defined by the two branches limiting the channel. This fact changes topology significantly and also the possibility for the latent heat to diffuse away.

Experiments in three dimensions to detect doublons and seaweed have been performed in a growth vessel with a volume of 100 cm^3 of pure liquid xenon. We use xenon as a transparent model substance for metals, because it forms a simple liquid, it crystallizes in an fcc-lattice, and it forms a solid-liquid interface which is rough at atomic scale. Details of the experimental setup are described in [16, 17]. At the beginning of the experiment the melt is brought to a homogeneous temperature T_∞ which is below the melting temperature, i.e. the melt is homogeneously undercooled. Then a crystal is nucleated in a capillary and grows through the capillary into the undercooled melt. The dimensions of the growth vessel are sufficiently large to ensure free growth of the crystal. According to the properties of the solid-liquid interface and the undercooling in the range of 10^{-3} to 10^{-2} in dimensionless units, a dendrite grows to a stationary state after several minutes and the temperature distribution around the dendrite reaches a steady state. An important feature of the experimental setup [17] is the possibility to shift this dendrite up and down inside of the growth vessel. Shifting the dendrite in the growth vessel means to disturb the temperature distribution around the crystal and to wash off the isotherms. Immediately after such a shift the crystal is surrounded by melt with a spatial homogeneous temperature. Any surface element of the dendrite tip is in contact with liquid at a temperature close to T_∞ . The thermal gradient at the crystal surface is everywhere the same. (Neglecting that the surface has been non isothermal before shifting the crystal.) Therefore any surface element of the crystal is growing with the same growth rate. This leads to an increase in the tip radius of the dendrite (Figure 1.) With increasing tip radius the dendrite reaches a state where the tip becomes unstable and tip splitting is observed. After tip splitting two tips continue to grow and form a doublon with a straight channel between the two tips. A sequence of contours is shown in Figure 1. By this procedure it is possible to grow various morphologies. Figure 2 shows a dendrite, a doublon and a seaweed morphology.

In difference to Brener et al. [11] we distinguish between doublon and seaweed morphology. This difference may originate from the three-dimensional geometry. The three morphologies can be distinguished from symmetry considerations: A dendrite shows a high degree of symmetry. For the seaweed no growth direction can distinguished in the plane of projection. The doublon has an axis of symmetry in the center of the channel.

In three dimensions the morphological transitions are not limited to the three cases shown in Figure 2. In addition to that we find triplons and quadruplons and

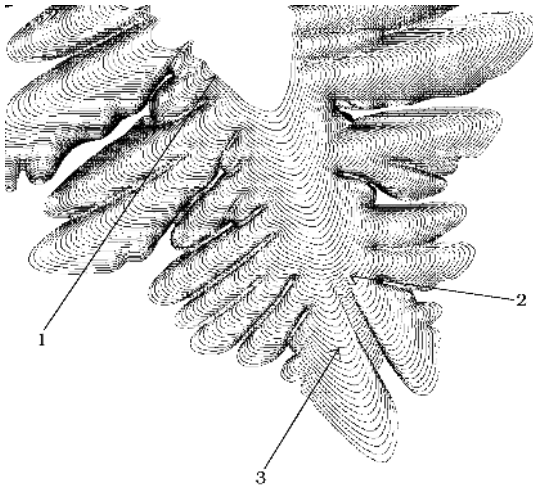


Fig. 1. A sequence of contours taken after the crystal has been shifted in the growth vessel. First we have the shape of the dendrite (arrow 1). During the temporal development the tip radius increases and the tip radius becomes unstable (arrow 2). Finally two tips are formed with a straight channel of liquid in between forming a doublon (arrow 3).

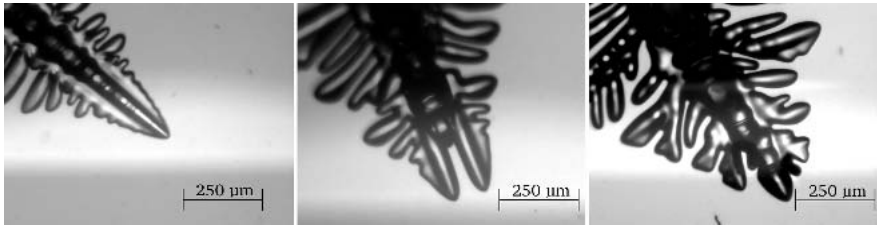


Fig. 2. Three morphologies: A dendrite, a doublon, and a seaweed.



Fig. 3. A crystal with three tips is formed in a similar process as observed in Figure 1.

even higher multiples of tips. Up to now we do not know the precise conditions for the occurrence of a special morphology. Figure 3 shows the development of a triplon out of a dendrite.

1.3 Numerical Studies

In order to verify and refine the qualitative analytical predictions by Brener et al. [11] we have performed phase field simulations with two different phase field models in 2D and 3D. Phase field models are an elegant approach to solve the analytical equations numerically. Instead of calculating a sharp phase boundary between solid and liquid in the Stefan- or sharp interface-problem every grid point holds in addition to the temperature also its phase state. The phase may have arbitrary values between 0 (solid) and 1 (liquid). A thin, but finite region of steep changes between solid and liquid models the interface. This width can be chosen and determines how well the approximation is in accordance with the sharp interface equations.

For our investigations we have chosen the models of Wheeler et al. [18] and Karma et al. [19]. The main difference between the two models is that in the Wheeler model the ratio between kinetic and capillary terms is fixed, where as in the Karma model the kinetic term can be cancelled by appropriately chosen terms for low undercoolings. We have performed simulations on a 2000×2000 grid with different undercoolings and anisotropies. The anisotropy axis goes from 0 to 6.5% as this is the maximal value where a crystal still grows in rough growth. For higher anisotropies the crystal becomes faceted as there occur forbidden growth directions. An initial coarse scan of 100 simulations was used to partition the plane. Subsequently a binary search for the morphology boundary was performed. By this refinement we were able to tie up the uncertainty region for the morphology boundary to up to $10^{-2}\%$. For lower undercoolings the simulation time increases significantly, therefore the uncertainty becomes bigger. In Figure 4 the results for the 2D simulations can be seen for both models. We have identified 3 regions of different morphologies: for low anisotropies seaweed structures (sw) and for high anisotropies dendrites are observed (den). For intermediate anisotropies and high enough undercoolings doublons are found (db). Both models show a similar behavior as the analytical predictions for the morphology boundary (seaweed-dendrite): The shape is concave for increasing anisotropy. However there is a big difference to the predictions for low undercoolings: while the predictions state that the whole shape of the boundary is concave we find in our simulations for low undercoolings and anisotropies a convex boundary. Comparing the two phase field models with each other we find qualitative correspondence. However we state that the boundary of the Karma model is slightly more on the left than the one of the Wheeler model. A detailed discussion of this behavior can be found in [20].

Three-dimensional simulations are very time-consuming. Even though we use an adaptive mesh code which runs parallel on 32 processors, it was not possible to obtain the same fine resolutions as for 2D simulations. As we have found qualitative agreement between the two models we have performed 3D simulations in a domain 400^3 only for the Karma model. The results are qualitatively similar to the 2D case however with two exceptions: i) The morphology boundary for the same parameters as in the 2D case is shifted along the anisotropy axis to the right by an amount of 0.32%. This result can be explained by the topological difference between 2D and

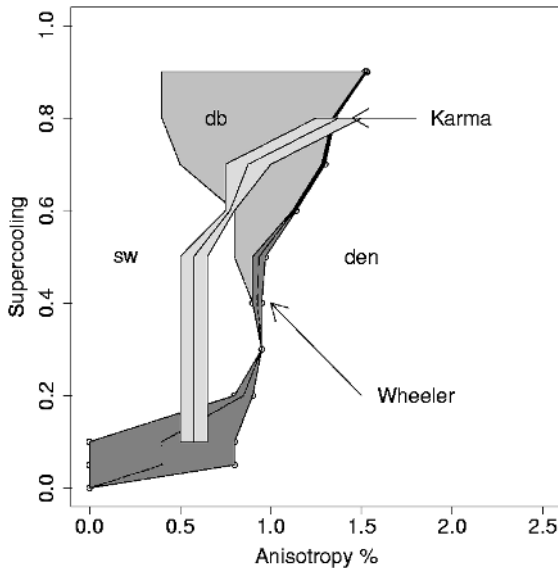


Fig. 4. Morphology diagram in 2 dimensions of the Wheeler model and the Karma model [20]. The zones marked with Wheeler and Karma correspond to the uncertainty regimes given by these models. The dendritic domain is denoted as “den”. Seaweed as “sw” and doublon as “db”.

3D: in 3D there is one additional dimension where heat can be transported away, therefore more anisotropy is needed to stabilize the structure to be dendritic. ii) No doublon region at all was found in 3D as opposed to 2D where we also started all simulations with the same initial conditions (a small spherical seed) and found a distinct doublon region. When starting with a spherical seed in 3D only seaweeds or dendrites can be simulated. It was however possible to simulate 3D doublons nevertheless by using special initial conditions [20]: by placing two identical seeds at a large enough distance, both start growing as a dendrite. However very soon they start interacting with each other and instead of developing four fins each they grow in parallel and develop only 3 fins each as observed in our experiments (Figure 3).

1.4

Conclusions

Quenching of metals during solidification provides some information on microstructures but not on the dynamics of morphology transitions during the solidification process. Transparent substances have been used to simulate solidification of metals. Rare gases have low melting entropy and form a „simple liquid“ similar to metals and can therefore be used as model substances to simulate transparent metals. In these systems the solidification process can be studied *in situ*. Up to now the in-

formation from model experiments with transparent model substances has been limited because no 3D information on the microstructure formed during solidification was available.

Two new features have been introduced into the study of solidification by model experiments: 1.) the study of various morphologies and morphological transitions, and 2.) the possibility to reconstruct the shapes of transparent 3D objects [21]. Morphology changes seem to lead to an explanation of grain refinement in metals, a feature that remained unexplained since a long time. The determination of the 3D shape of objects formed during freezing provides for the first time the possibility to determine 3D shape parameters necessary to apply theories in industrial processes. We have started to determine such parameters and to characterize various morphologies formed during solidification and their transitions. We have the unique possibility to combine theoretical studies with experiments.

The interaction of experiment and theory is crucial. Theoretical studies are stimulated by unexpected experimental observations, and using an expression coined by L. Pasteur, the eye of the experimentalist is trained by theoretical results to see new structures.

Acknowledgements

We thank Professor Dr. H. R. Ott for his support of our experiments. This work was supported by the Swiss National Science Foundation.

References

- [1] J.P. GOLLUB and J.S. LANGER, *Rev. Mod. Phys.* 1999, 71, S396-S403
- [2] A. KARMA in *Banching in Nature* (Ed.: V. Fleury, J.-F. Gouyet, and M. LEONETTI) Springer, Berlin, 2001, Chapter 9
- [3] K. DRAGEVSKI, R. F. COCHRANE, and A.M. MULLIS, *Phys. Rev. Lett.* 2002, 89, 215502
- [4] R. WILLNECKER, D.M. HERLACH, and B. FEUERBACH, *Appl. Phys. Lett.* 1990, 56, 324–326
- [5] M. SCHWARZ, A. KARMA, K. ECKLER, and D.M. HERLACH, 1994, 73, 1380–83
- [6] M. BEN AMAR and E. BRENER, *Phys. Rev. Lett.* 1995, 75, 561–564
- [7] T. IHLE, and H. MÜLLER-KRUMBHAAR, *Phys. Rev. Lett.* 1993, 70, 3083–86
- [8] T. ABEL, E. BRENER, and H. MÜLLER-KRUMBHAAR, *Phys. Rev. E*, 1997, 55, 7789–92
- [9] T. IHLE, *Wachstumsmuster unter diffusivem Transport*, Berichte des Forschungszentrums Jülich, Jülich, 1996, Vol.3230,
- [10] E. BRENER, H. MÜLLER-KRUMBHAAR, and D. TEMKIN, *Phys. Rev. E*, 1996, 54, 2714–22
- [11] E. BRENER, H. MÜLLER-KRUMBHAAR, D. TEMKIN, and T. ABEL, *Physica A* 1998, 249, 73–81
- [12] R.H. MATHIESSEN, L. ARNBERG, K. RAMSOSKAR, T. WEITKAMP, C. RAU, and A. SNIGIREV, *Metall. Mater. Trans. B*, 2002, 33B, 613–623
- [13] S. AKAMATSU, G. FAIVRE, and T. IHLE, *Phys. Rev. E* 1995, 51, 4751–73
- [14] M.B. KOSS, J.C. LACOMBE, L.A. TENNENHOUSE, M.E. GLICKSMAN, and E.A. WINSA, *Metall. Mater. Trans. A*, 1999, 30A, 3177–90.

- [15] D. P. CORRIGAN, K. B. KOSS, J.C. LA-COMBE, K.D. DE JAGER, L.A. TENNENHOUSE, and M.E. GLICKSMAN, *Phys. Rev. E*, 1999, 60, 7217–7223
- [16] U. BISANG and J.H. BILGRAM, *Phys. Rev. E*, 1996, 54, 5309–26
- [17] I. STALDER and J.H. BILGRAM, *Europhys. Lett.* 2001, 56, 829–835
- [18] A.A WHEELER, B.T. MURRAY and R.J. SCHAEFER, *Physica D*, 1993, 66 , 243–262
- [19] A. KARMA and W.-J. RAPPEL, *Phys. Rev. E* 1998, 57 , 4323–49
- [20] H.M. SINGER, I. LOGINOVA, J.H. BILGRAM, and G. AMBERG, *J. Cryst. Growth*, submitted
- [21] H.M. SINGER and J.H. BILGRAM, this volume

2

Thermal Roughening of a Solid-on-Solid Model with Elastic Interaction

FRANK GUTHEIM, HEINER MÜLLER-KRUMBHAAR, EFIM BRENER and CHRISTOPH PÜTTER

2.1

Introduction

At low temperatures crystal surfaces are known to assume the shape of a plane facet. With increasing temperature, fluctuations gradually contribute a nonzero thickness to the initially flat facet. This surface thickness finally diverges at a finite temperature, the roughening temperature, where the order of the facet is lost completely. For kinetics of crystal growth and solidification, the roughening transition plays a decisive role. This transition can be described by a set of renormalization group equations first analyzed by Kosterlitz and Thouless [1]. Because of its unusual properties and the relation to the two-dimensional Coulomb gas, this roughening transition has attracted substantial attention.

Various discrete solid-on-solid (SOS) models have been shown to undergo this type of transition. Most of these models incorporate local interactions, at most next-nearest neighbor interactions. Within some of these models a transition involving in-plane disorder is possible, usually referred to as preroughening.

Interaction of surface defects by means of elastic deformation of the crystal, however, is of a long-ranged nature and has apparently not been previously studied in the context of roughening. Leaving the matter of preroughening aside, we will try to elucidate the effects of long-range elastic interactions on the roughening process.

2.2

Step Interaction

Elastic step interaction on the surface of a semi-infinite crystal can be described in terms of elastic force dipoles located at the step edges. Using symmetry arguments one can determine two types of force dipoles that are considered to be present at a step. One type involves in-plane forces perpendicular to the step, the other arises from forces orthogonal to the crystal surface. The former leads to attractive or repulsive interaction depending on the signs of the steps, the latter produces a sign-independent behavior,

which is strictly repulsive. There are materials where the sign-dependent contributions are small compared to the step repulsion caused by in-plane forces. Thus we restrict our model to the case, where we can neglect sign-dependence of the steps [2]. We can make another simplification of the step-step interaction by assuming a scalar $w \sim 1/r^3$ interaction associated with isotropic dipoles at the step. From this, the energy per unit length of the line for a configuration with two parallel steps at distance d is just

$$\tilde{W}_{\text{scalar}} = 4\gamma \frac{1}{d^2} + 2\gamma \frac{1}{\varepsilon^2}, \quad (1)$$

where the interaction is limited to distances greater than ε . The factor γ is given by

$$\gamma = \frac{1 - \sigma^2}{\pi E} Q^2, \quad (2)$$

where Q is the dipole moment per unit length of the step, σ the Poisson ratio and E Young's modulus.

2.3

Model Description

Within the framework of a solid-on-solid model we describe the crystal surface by a simple height field h_i of integer multiples of the lattice constant a . Like in a common SOS model, overhangs are forbidden. We define an elastic step interaction by introducing a field of elastic dipole charges q . To every lattice site k a dipole charge q_k proportional to the number of height differences to the four neighboring sites is assigned. The elastic dipole charges interact, in consequence of Eq. (1), via a modified r^{-3} interaction potential $\Psi_{p_{\max}, l}(r)$,

$$\Psi_{p_{\max}, l}(r) = \begin{cases} \min((a/r)^3, p_{\max}) & \text{if } r \leq l \\ 0 & \text{if } r > l \end{cases} \quad (3)$$

where r is the in-plane distance between two lattice sites and p_{\max} is a number limiting the interaction potential in vicinity of $r = 0$. We also introduce the cutoff length l , i. e., the potential vanishes for distances greater than l . This gives rise to the elastic energy

$$E_{\text{el}} = \frac{w_{\text{el}}}{2} \sum_{i,j} q_i q_j \Psi_{p_{\max}, l}(r_{ij}), \quad (4)$$

where r_{ij} is the distance between lattice sites i and j and w_{el} can be adjusted to give the desired interaction strength. Note that the case $i = j$ is not excluded from the summation. For two straight steps of length L with distance d and without cutoff this elastic energy contribution consists of the self energies of the steps and the expected $\sim d^{-2}$ step interaction term

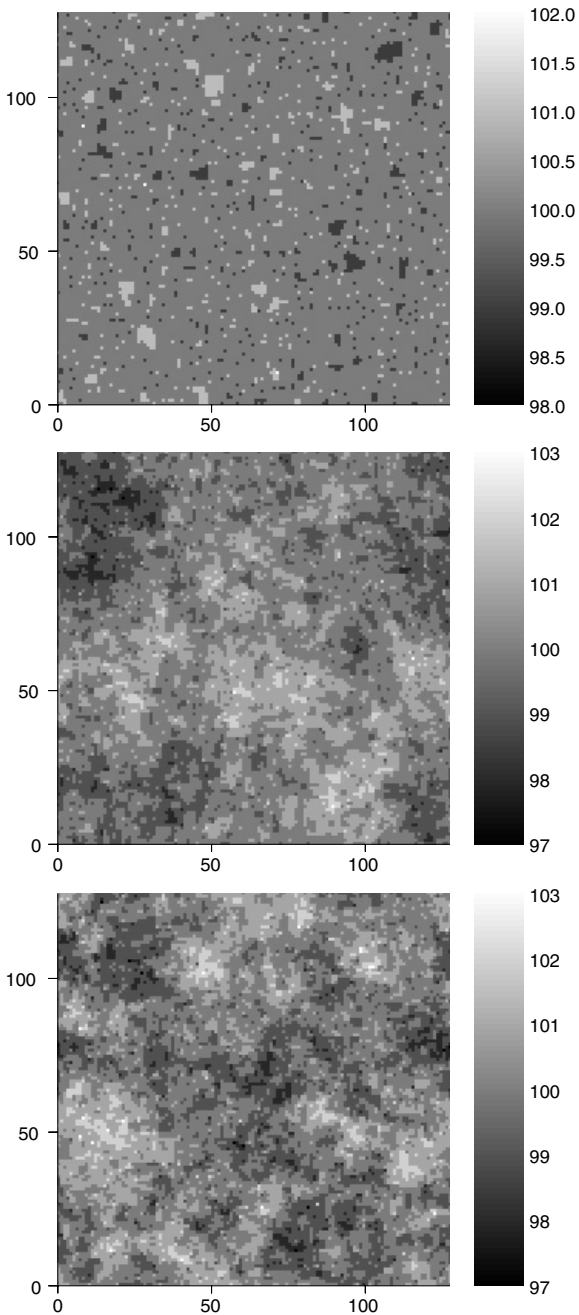


Fig. 1 Roughening transition of a surface under elastic interaction without cutoff. The height field of our model for three different configurations, $T \approx 4.5 w_{el}$, $T \approx 13 w_{el}$ (top to bottom), are shown as topviews. The heights are coded in grayscales. The average height corresponds to 100 atomic units.

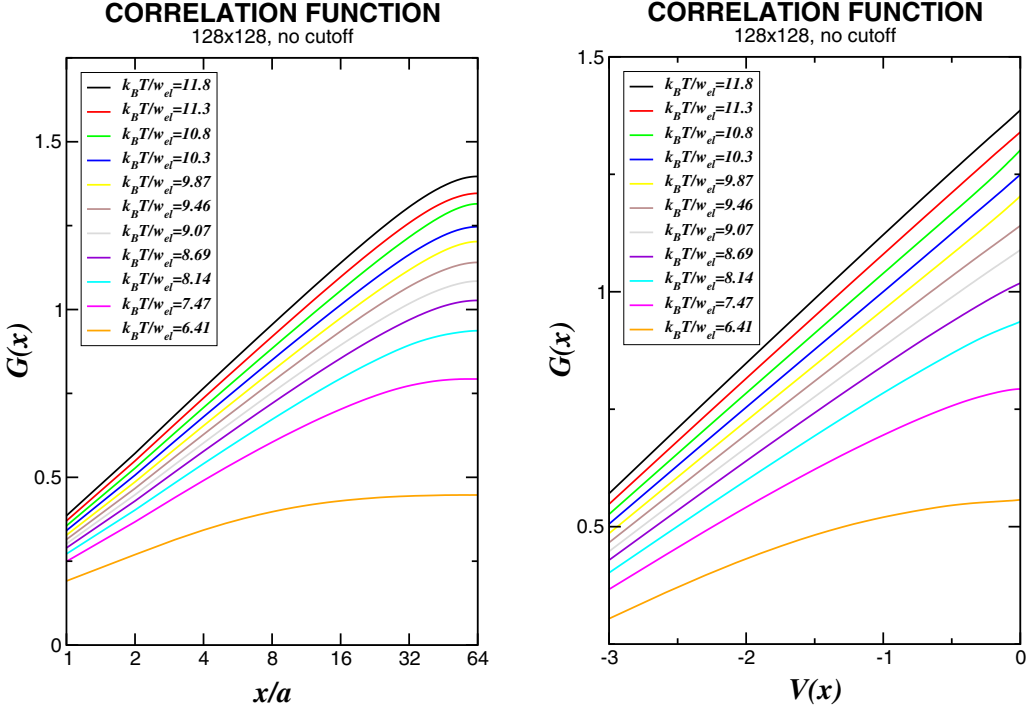


Fig. 2 Height-height correlation function without cutoff along the main directions of the lattice. Left: The correlation function saturates for all temperatures due to the finite size of the system. Right: Same plot, but with finite size correction [2]. The correlation function saturates for small temperatures and shows logarithmic behavior for $T \geq T_R$. The first straight line gives an estimate of $k_n T_R/w_{el} \approx 9.0$.

$$E_{\text{int}} \approx 8 w_{\text{el}} \frac{L}{d^2}, \quad (5)$$

for large distances $d \gg a$.

Modifying p_{max} the self energy contribution of a straight step can be adjusted to the desired line energy, independently of the step-step interaction amplitude.

For given p_{max} the relative amplitude of line energy and step-step interaction is fixed and we can concentrate on the crossover from a local to a long-range model depending on the cutoff length l , which is studied using the interaction potentials $\Psi_{1,l}$ where $p_{\text{max}} = 1$. Later, however, other relative amplitudes are studied for the potential $\Psi_{p_{\text{max},\infty}}$ without cutoff.

The simulation is carried out on a square lattice of size $(L/a)^2 = 64 \times 64$ to 128×128 . In order to calculate the difference in energy for every metropolis Monte Carlo trial, we apply a multigrid scheme based on Ref. [3], which reduces computational cost and which has already been applied successfully to submonolayer epitaxy [4].